Title
Burst delay line for generating ultrashort pulse bursts with interval tunability from femtoseconds to nanoseconds.

Journal
Optics Letters, 51(11)

ISSN
0146-9592

Authors
Shimada, Keitaro
Korakis, Vasileios
Chirinos, Jose
et al.

Publication Date
2026-06-01

DOI
10.1364/ol.592952

Optics Letters

Burst delay line for generating ultrashort pulse bursts with interval tunability from femtoseconds to nanoseconds

KEITARO SHIMADA,[1,2] VASILEIOS KORAKIS,[2,3] JOSE CHIRINOS,[2] XIANGLEI MAO,[2] AND VASSILIA ZORBA[2,3,*]

[1]Department of Bioengineering, The University of Tokyo, Tokyo 113-8656, Japan
[2]Energy Technologies Area, Lawrence Berkeley National Laboratory, Berkeley, California 94720, USA
[3]Department of Mechanical Engineering, University of California at Berkeley, Berkeley, California 94720-1740, USA
*vzorba@lbl.gov

Received 9 February 2026; revised 6 May 2026; accepted 7 May 2026; posted 8 May 2026; published 27 May 2026

Ultrashort burst laser pulses are important for applications in laser processing and spectroscopy. However, existing burst generators face limitations in pulse time interval tunability and coaxiality. Here, we present a burst pulse generator that delivers coaxial ultrashort pulses with tunable pulse time intervals using a single translation stage. The constructed system produced eight femtosecond pulses with uniform intervals tunable from 100 fs to 1.93 ns, equivalent to burst-internal repetition rates spanning 10 THz to 0.52 GHz. We further demonstrated interval-dependent plasma emission in air filamentation, providing a compact platform to study burst-laser–induced phenomena.

https://doi.org/10.1364/OL.592952

Ultrafast laser–matter interactions involve processes on femtosecond to nanosecond timescales, including carrier excitation, electron–phonon coupling, lattice heating, plasma expansion, and shockwave generation [1,2]. Burst pulses provide a way to couple selectively to these dynamics, and the pulse time interval is therefore a critical parameter [3]. At sub-picosecond to few-picosecond delays, pulses interact with carriers before equilibration with the lattice, enabling coherent excitation such as optical phonons and terahertz emission [4]. At picoseconds to tens of picoseconds, interactions with melt formation and early plasma expansion can influence surface morphology and induce regular periodic surface structures [5,6]. At hundreds of picoseconds to nanoseconds, pulses couple to slower responses: during thermal relaxation, they can drive ablation cooling and enhance material removal efficiency [7,8], interaction with the expanding plasma can increase emission signals in laser-induced breakdown spectroscopy (LIBS) [9], coupling to the hydrodynamic response can reinforce shockwaves [10], and appropriately timed pulses can facilitate discharge guiding [11]. These examples show that diverse applications, including laser processing, LIBS, discharge guiding, and phonon excitation, are strongly dependent on the pulse time interval, highlighting the importance of sources that can tune delays from femtoseconds to nanoseconds.

The generation of burst pulses can be broadly divided into two approaches. The first relies on controlling the repetition rate of the seed laser using modulators such as electro-optic or acousto-optic devices, followed by amplification [12,13]. This technique has been widely applied in industrial laser systems. However, the achievable control over the pulse time interval and pulse energy is restricted by distortions introduced in the gain medium and the risk of optical damage during amplification. The second approach is based on shaping a single femtosecond pulse into multiple sub-pulses using free-space optics [14–21]. Various schemes have been demonstrated, including Fabry–Perot cavities [14,15], free-space delay loop [16], free-space angular-chirp-enhanced delay [17], and spectrum shuttle [18]. These methods can generate bursts with adjustable intervals and coaxial output, although they generally face difficulties in achieving pulse time intervals shorter than about 10 ps. Other free-space designs, such as Deathstar [19] and dual parallel reflection [20], can extend the interval from the femtosecond to the nanosecond regime. However, the pulses emerge from different spatial positions and are therefore not coaxial. Multiple Michelson interferometers [21] can provide coaxial ultrashort bursts with femtosecond-to-picosecond intervals. However, extension to the nanosecond regime requires long delay paths exceeding a meter, and the use of multiple interferometer stages demands independent tuning for each stage, which complicates operation. A compact comparison of these methods is provided in Supplement 1 and Table S1.

In this Letter, we present a burst delay line (BDL) that provides coaxial ultrashort pulse bursts with interval tunability from femtoseconds to nanoseconds, corresponding to pulse-to-pulse repetition rates spanning the terahertz (THz)-to-gigahertz (GHz) range. In the BDL, multiple Michelson geometries are combined so that each pulse undergoes a different number of round trips through a single translation stage, enabling adjustment of the pulse time interval by operating only one stage. Using this configuration, we generated an eight-pulse burst with femtosecond pulse duration and demonstrated tunability of the

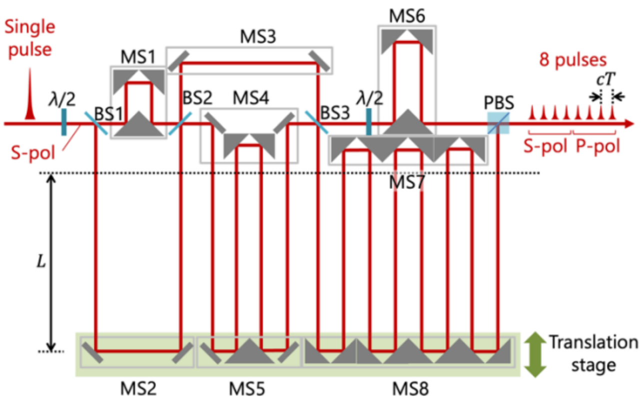

Fig. 1. Schematic of a burst delay line (BDL) for generating eight-pulse bursts. $\lambda/2$, Half-wave plate; BS1–3, beam splitter 1–3; MS1–8, Mirror set 1–8; PBS, polarizing beam splitter. The dotted line marks the reference stage position for equal optical paths.

pulse time interval across the femtosecond–nanosecond range. Furthermore, we applied the system to investigate pulse time interval-dependent side plasma emission in air filamentation induced by burst pulses. The BDL provides a versatile platform for investigating interval-dependent ultrafast phenomena across multiple regimes of light–matter interaction.

Figure 1 shows a schematic of the BDL for generating eight-pulse bursts. The system consists of two half-wave plates, three beam splitters (BS1–3), a polarizing beam splitter (PBS), and multiple mirrors, which are grouped into eight mirror sets (MS1–8) for clarity. A single input pulse is first adjusted by a half-wave plate so that the pulses are S-polarized at BS1–3. At BS1, one path passes through the delay implemented by MS1 before reaching BS2, while the other path is reflected by MS2 on the translation stage and then directed to BS2. At BS2, the pulse is again divided: one path passes through MS3 before reaching BS3, and the other undergoes two round trips between MS4 on the fixed mount and MS5 on the translation stage before entering BS3. At BS3, the pulse is further divided: one path passes through MS6 before reaching the PBS, while the other undergoes four round trips between MS7 on the fixed mount and MS8 on the translation stage before arriving at the PBS. By rotating the polarization of one path with a half-wave plate, the PBS finally combines all eight pulses into a coaxial output.

In this configuration, the round-trip paths are arranged parallel to the translation stage motion. The delays of MS1, MS3, and MS6 are designed such that, at a specific reference position of the translation stage, the two optical paths at each of the three splitting points are equal. Consequently, the eight pulses experience different numbers of round trips (0–7) between the stage-mounted and fixed mirrors, and the resulting pulse time interval T depends on the stage displacement L from the reference position as

$$T = \frac{2L}{c}, \quad \textbf{(1)}$$

where c is the speed of light. Thus, by translating the stage over distances ranging from tens of micrometers to hundreds of millimeters, the BDL enables tuning of the output burst pulse interval from the hundreds of femtoseconds to the nanosecond regime. The pulse duration of the output burst is affected by the positive dispersion of the BDL. By using negatively pre-chirped input pulses, the output pulses can be temporally compressed, allowing the generation of ultrashort burst pulses. The relative intensity of each output pulse with respect to the incident pulse, referred to here as the throughput per pulse, is determined by the splitting ratios of the beam splitters together with the transmission and reflection losses of the optical components. The throughput I_k/I_{in} for the k-th pulse can be expressed as

$$I_k/I_{\mathrm{in}} = \left[\prod_{i=1}^{3} C_i\left(\mathrm{BS}_i\left(k\right)\right)\right]\Lambda_k. \quad \textbf{(2)}$$

Here, $C_i\left(\mathrm{BS}_i\left(k\right)\right)$ represents the transmission or reflection coefficient of BSi depending on whether the k-th pulse is transmitted (T_i) or reflected (R_i). The sequence of transmission/reflection at BS1–3 for the eight pulses is given as follows: pulse 1 (T–R–R), pulse 2 (R–T–R), pulse 3 (T–T–T), pulse 4 (R–R–T), pulse 5 (T–R–T), pulse 6 (R–T–T), pulse 7 (T–T–R), and pulse 8 (R–R–R). Λ_k denotes the cumulative loss of all other optical components along the path of the k-th pulse, including the mirrors, the half-wave plates, and the PBS. With 50:50 beam splitters and low-loss optics, the BDL enables efficient generation of uniform-intensity burst pulses with high throughput. In the output burst, pulses 1–4 are P-polarized and pulses 5–8 are S-polarized with respect to the PBS. The BDL can be extended to 16 pulses by adding one splitting stage, although scalability is limited by alignment sensitivity, optical loss, and dispersion.

We constructed the BDL within a footprint of 450 mm × 700 mm. To provide flexibility with respect to the source wavelength, the system was designed to operate at both 800 nm and 1030 nm by replacing only the half-wave plates (WPH10M-808 or WPH10M-1030, Thorlabs). For S-polarized input, the beam splitters BS1–3 (BSS11R, Thorlabs) were measured to have transmission/reflection ratios of 60%/40% at 800 nm and 61%/39% at 1030 nm. The PBS (PBS252, Thorlabs) was used to combine the pulses coaxially. The mirrors in MS1–8 were protected silver mirrors, including a plane mirror (PF10-03-P01, Thorlabs), a right-angle prism mirror (MRAK25-P01, Thorlabs), and a roof mirror (HRS1015-P01, Thorlabs). The current optics support approximately 700–1050 nm; replacing the BS, PBS, and half-wave plates could extend the reflective BDL geometry over the 450 nm–2 µm mirror range. The translation stage was a 300 mm linear stage (DDS300, Thorlabs), and the delays of MS1, MS3, and MS6 were adjusted so that $T = 0$ corresponded to a stage position 10 mm from one end, allowing a maximum travel of $L = 290$ mm ($T = 1.93$ ns). As light sources, we used a mode-locked Ti:sapphire laser with a chirped pulse amplifier system (Astrella-USP-1K, Coherent), operated at 100 Hz and a central wavelength of 800 nm with a negatively chirped pulse duration stretched from 40 fs to 260 fs, and a Yb-based laser (Tangor, Amplitude), operated at 200 kHz and at 1030 nm with a compressed pulse duration of 500 fs.

We first evaluated the tunability of the pulse time interval using the 800 nm wavelength band. The interval T was varied by adjusting the translation stage displacement L. For $T \geq 50$ ps, the time intervals were measured with a 1.2-GHz photodiode (818-BB-21, Newport) and an 8-GHz oscilloscope (MSO64, Tektronix). For $T \leq 20$ ps, the time intervals were determined using frequency-resolved optical gating (FROG) with a temporal resolution of 10 fs. In the FROG measurements, two pulses were selected at a time, and their separation was measured. By repeating this procedure, the intervals among all eight pulses were obtained. As shown in Fig. 2, the measured pulse intervals from 100 fs to 1.93 ns agreed well with the theoretical line

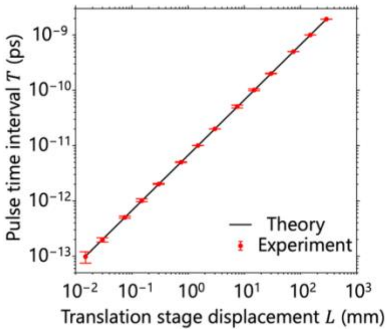

Fig. 2. Pulse time intervals T varied by adjusting the translation stage displacement L. The error bars indicate the minimum and maximum values of the intervals among the eight pulses.

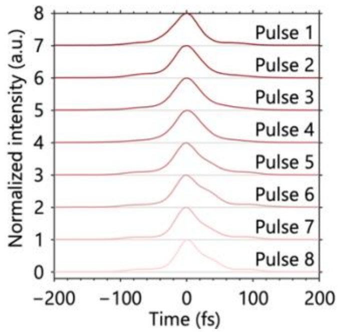

Fig. 3. Temporal waveforms of the eight pulses measured at 800 nm.

calculated using Eq. (1). This corresponds to pulse-to-pulse repetition rates from 10 THz down to 0.52 GHz. From the specified bidirectional repeatability of the translation stage (±0.25 μm), the pulse-interval repeatability was estimated to be ±1.7 fs.

We next evaluated the pulse duration of the compressed burst pulses. Using negatively chirped input pulses at the 800 nm wavelength band, we demonstrated the generation of compressed burst pulses. The temporal profiles of the eight pulses were independently retrieved using a FROG (Fast FROG PS1, Femto Easy). The obtained waveforms are shown in Fig. 3, confirming that ultrashort burst pulses with an FWHM duration of 49.0 ± 3.0 fs were achieved. The small pulse-to-pulse waveform differences in Fig. 3 are attributed to residual path-dependent spectral amplitude and phase variations; nevertheless, dispersion arising from different BS transmissions was estimated to cause less than 1% temporal broadening for the measured 50-fs pulses.

We next evaluated the throughput per pulse at both 800 nm and 1030 nm wavelength bands. The energies of the incident and output pulses were measured with energy meters (PE10-C, Ophir, for 800 nm; FL250A-BB-35, Ophir, for 1030 nm), and the throughput per pulse was calculated. The results are shown in Fig. 4, together with the theoretical values calculated using the measured transmission/reflection ratio of the BSs and the manufacturer-specified losses of the mirrors and PBS, demonstrating good agreement. The variation in throughput among the pulses originates from the transmission and reflection ratios of the beam splitters; pulse 3 is higher because it follows the T–T–T path for a 60%/40% splitting ratio. The overall throughput was 48% at 800 nm and 53% at 1030 nm. The

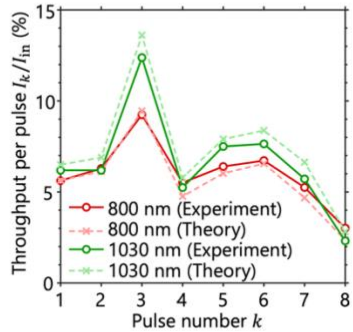

Fig. 4. Throughput per pulse at 800 nm and 1030 nm.

optical loss mainly arose from multiple reflections at the mirrors (reflectivity 95–97%), which could be improved by employing mirrors with higher reflectivity.

At 800 nm, the output pulses showed near-field centroid shifts within ±500 μm and pointing angles within ±150 μrad over the full tuning range (see Supplement 1, Fig. S1). We then demonstrated the applicability of the BDL to the investigation of interval-dependent phenomena by exploiting its ability to deliver coaxial ultrashort burst pulses with tunable pulse time intervals from the femtosecond to nanosecond regime. As a representative example, we formed air filamentation with burst pulses and spectrally measured the plasma emission. Filamentation is a highly nonlinear process that is sensitive to pulse-to-pulse timing, and this demonstration highlights the potential of the BDL for systematically probing interval-dependent plasma dynamics. Using the 800 nm wavelength band, eight pulses with a total energy of 2.2 mJ were focused by a 150 mm focal length lens, as shown in Fig. 5(a). Side plasma emission was collected by a 24 mm focal length lens and detected with a spectrometer (IsoPlane, Princeton Instruments) with a gate width of 20 ns. The pulse time interval was varied from 0 to 1933 ps on a logarithmic scale, and for each interval, 10^5 shots were acquired in synchronization with the 100 Hz laser repetition rate. Here, $T = 0$ ps denotes the nominal zero-delay position extrapolated from the measured $T = 100$ fs condition, where pulses may overlap coherently or nonlinearly. Only the pulse interval was intentionally varied; pulse-to-pulse waveform and peak-intensity differences may affect absolute emission intensities but were not independently controlled.

Figure 5(b) shows the side emission spectra of filamentation generated by eight pulses for different pulse time intervals. In the measured range of 320–480 nm, the emission exhibited strong dependence on the interval. The 391 nm line from ionized nitrogen was strongest at 20–500 ps, when the subsequent pulses interact with a plasma of high electron density, enhancing ionic excitation. In contrast, the 337 nm line attributed to neutral nitrogen became prominent at 500–1000 ps, where plasma expansion and reduced electron temperature favor neutral-state emission. Furthermore, a broad continuum appeared in the longer-wavelength region around 200–500 ps, which can be attributed to recombination radiation and electron–ion bremsstrahlung in the well-developed plasma. To further examine the interval dependence, Figs. 5(c) and 5(d) compare the emission intensities at 337 nm and 391 nm for eight pulses, four pulses (pulses 1–4), and two pulses (pulses 1 and 2). Although the overall dependence was similar irrespective of the number of pulses, the interval dependence became more pronounced as the number

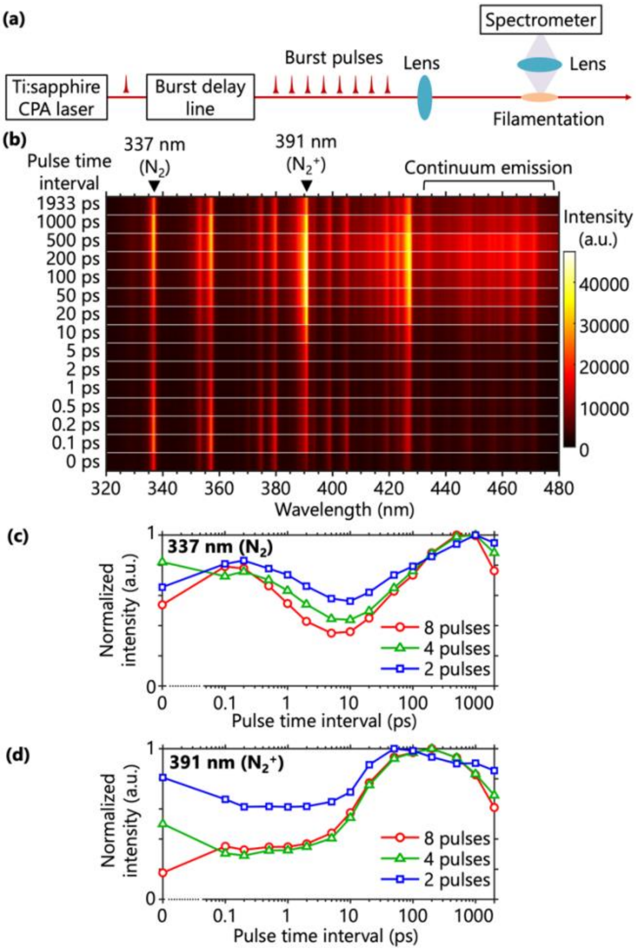

Fig. 5. Interval-dependent plasma emission from air filamentation induced by burst pulses. (a) Experimental setup. (b) Side emission spectra obtained with eight pulses at varying pulse time intervals. (c) Normalized emission intensity at 337 nm and (d) at 391 nm as a function of the pulse time interval for eight, four, and two pulses.

of pulses increased. These results demonstrate that by adjusting the pulse time interval, the emission of specific species can be selectively enhanced. Such controllability suggests potential applications in remote atmospheric sensing, where selective enhancement of molecular or ionic emission lines is valuable, as well as in plasma-based light sources and filament-assisted discharge guiding.

In this study, we developed a burst delay line (BDL) capable of generating coaxial ultrashort pulse bursts with tunable pulse time intervals from the femtosecond to nanosecond regime, corresponding to THz-to-GHz pulse-to-pulse repetition rates. We verified its performance through measurements of interval scaling, pulse duration, and throughput, and we demonstrated its applicability in air filamentation by resolving interval-dependent plasma emission. The ability to flexibly tailor the pulse time interval while preserving ultrashort duration makes the BDL a powerful tool for burst-laser–induced phenomena. In particular, it opens new possibilities for applications in laser processing and manufacturing, where ablation efficiency and surface quality depend strongly on pulse timing, and in laser-induced breakdown spectroscopy, where selective enhancement of molecular and ionic emission lines is valuable. More broadly, it provides a compact platform for advancing ultrafast science and technology across diverse light–matter interactions.

Funding. U.S. Department of Energy, National Nuclear Security Administration, Office of Defense Nuclear Nonproliferation (DE-AC02-05CH11231); Japan Science and Technology Agency (JPMJAX22K8).

Disclosures. The authors declare no conflicts of interest.

Data availability. Data underlying the results presented in this paper are not publicly available at this time but may be obtained from the authors upon reasonable request.

Supplemental document. See Supplement 1 for supporting content.

REFERENCES

1. R. E. Russo, X. Mao, J. J. Gonzalez, *et al.*, Anal. Chem. **85**, 6162 (2013).
2. B. Rethfeld, D. S. Ivanov, M. E. Garcia, *et al.*, J. Phys. D Appl. Phys. **50**, 193001 (2017).
3. D. J. Förster, B. Jäggi, A. Michalowski, *et al.*, Materials **14**, 3331 (2021).
4. T. Feurer, J. C. Vaughan, and K. A. Nelson, Science **299**, 374 (2003).
5. F. Fraggelakis, G. Mincuzzi, J. Lopez, *et al.*, Appl. Surf. Sci. **470**, 677 (2019).
6. Y. Zhang, Q. Jiang, K. Cao, *et al.*, Photonics Res. **9**, 839 (2021).
7. C. Kerse, H. Kalaycıoğlu, P. Elahi, *et al.*, Nature **537**, 84 (2016).
8. M. Park, Y. Gu, X. Mao, *et al.*, Sci. Adv. **9**, eadf6397 (2023).
9. V. I. Babushok, F. C. DeLucia, J. L. Gottfried, *et al.*, Spectrochim. Acta B **61**, 999 (2006).
10. Y. Kai, J. Lem, M. Ossiander, *et al.*, Opt. Express **31**, 31308 (2023).
11. P. Polynkin, Appl. Phys. Lett. **111**, 161102 (2017).
12. Y. Liu, J. Wu, X. Wen, *et al.*, Opt. Express **28**, 13414 (2020).
13. T. Bartulevicius, M. Lipnickas, V. Petrauskiene, *et al.*, Opt. Express **30**, 36849 (2022).
14. A. Okhrimchuk, S. Fedotov, I. Glebov, *et al.*, Sci. Rep. **7**, 16563 (2017).
15. L. Dresselhaus-Cooper, J. E. Gorfain, C. T. Key, *et al.*, Sci. Rep. **9**, 3689 (2019).
16. Z. Xu, X. Liu, Y. Liao, *et al.*, Appl. Opt. **61**, 8641 (2022).
17. J.-L. Wu, Y.-Q. Xu, J.-J. Xu, *et al.*, Light Sci. Appl. **6**, e16196 (2017).
18. K. Shimada, A. Ishijima, T. Saiki, *et al.*, Adv. Photon. Nexus **3**, 016002 (2023).
19. C. Klieber, E. Peronne, K. Katayama, *et al.*, Appl. Phys. Lett. **98**, 211908 (2011).
20. R. Tanaka, K. Shimada, A. Ishijima, *et al.*, Opt. Lett. **50**, 2906 (2025).
21. B. Zhou, H. Cheng, M. J. Soileau, *et al.*, Appl. Opt. **60**, 5867 (2021).